








# Continuous polymer films deposited on top of porous substrates using plasma-enhanced atomic layer deposition and molecular layer deposition

Cite as: J. Vac. Sci. Technol. A 38, 052409 (2020); doi: 10.1116/6.0000271

Submitted: 19 April 2020 · Accepted: 21 July 2020 ·

Published Online: 24 August 2020



Brian C. Welch,<sup>1</sup>  Olivia M. McIntee,<sup>1</sup>  Anand B. Ode,<sup>2</sup>  Bonnie B. McKenzie,<sup>3</sup>  Alan R. Greenberg,<sup>1,4</sup>   
Victor M. Bright,<sup>1</sup>  and Steven M. George<sup>2</sup> 

## AFFILIATIONS

<sup>1</sup>Department of Mechanical Engineering, University of Colorado, Boulder, Colorado 80309

<sup>2</sup>Department of Chemistry, University of Colorado, Boulder, Colorado 80309

<sup>3</sup>Sandia National Laboratories, Albuquerque, New Mexico 87185

<sup>4</sup>Membrane Science, Engineering and Technology Center, University of Colorado, Boulder, Colorado 80309

**Note:** This paper is part of the 2021 Special Topic Collection on Atomic Layer Deposition (ALD).

## ABSTRACT

Molecular layer deposition (MLD) is able to produce ultrathin polymer films with control over thickness, cross-linking, and chemical composition. With these capabilities, MLD should be useful in the fabrication of novel polymer membranes on porous supports. However, confining a continuous MLD film to the surface of porous substrates is difficult because of MLD film growth in the pores. The deposition in the pores lowers the conductance of the porous support. This paper presents a method to deposit continuous polymer films on top of porous substrates. In this method, Al<sub>2</sub>O<sub>3</sub> plasma-enhanced atomic layer deposition (PE-ALD) using trimethylaluminum and oxygen plasma as the reactants was first used to cap the pores of the substrate. Subsequently, a polyamide MLD film was deposited on the Al<sub>2</sub>O<sub>3</sub> PE-ALD capping layer using *m*-phenylenediamine and trimesoyl chloride as the reactants. The Al<sub>2</sub>O<sub>3</sub> pore caps were then removed from the porous substrate by etching from the backside using a timed exposure to a dilute sodium hydroxide solution. This method was demonstrated using anodic aluminum oxide (AAO) and polyethersulfone (PES) porous substrates. Al<sub>2</sub>O<sub>3</sub> PE-ALD film growth was limited to the top of the porous substrate, resulting in rapid surface recombination or high sticking coefficients for the reactive plasma species within the pores. Gas permeance measurements confirmed the pore capping of the AAO substrates. The reopening of the pores by dissolving the Al<sub>2</sub>O<sub>3</sub> pore caps with a sodium hydroxide solution was monitored using gas permeance versus etch time. The removal of the Al<sub>2</sub>O<sub>3</sub> pore caps from the PES substrates could also dissolve the Al<sub>2</sub>O<sub>3</sub> layer underneath the MLD film. The loss of this Al<sub>2</sub>O<sub>3</sub> layer led to the detachment of the MLD film from the PES substrate. However, the MLD film could be anchored to the PES support at fractures located in the Al<sub>2</sub>O<sub>3</sub> film prior to the MLD. The Al<sub>2</sub>O<sub>3</sub> film fracture allowed the MLD film to anchor firmly to the PES substrate by MLD in the pores of the PES porous substrate. The distance between the anchor points was a function of fracture density. This distance could be controlled by applying a tensile stress to the Al<sub>2</sub>O<sub>3</sub> PE-ALD film to fracture the film through sample bending. This method produced firmly anchored polymer MLD films on top of the PES porous substrates.

Published under license by AVS. <https://doi.org/10.1116/6.0000271>

## I. INTRODUCTION

Molecular layer deposition (MLD) is a thin film deposition technique that allows for nanometer-scale control over the thickness of the deposited polymeric layer.<sup>1–3</sup> MLD uses sequential, self-limiting surface reactions to deposit organic and hybrid organic-inorganic films.<sup>4</sup> MLD is analogous to atomic layer deposition (ALD) and can

deposit polymeric films with conformality and atomic layer control.<sup>5</sup> MLD processing has the potential to produce polymer films with a thickness of only a few nanometers while maintaining a high level of control over chemical composition and properties.<sup>6,7</sup>

MLD films can be useful for the fabrication of polymer membranes.<sup>8,9</sup> An extremely thin polymer MLD layer can be deposited such that the thin film-porous substrate combination provides a

functional high performance membrane.<sup>10–14</sup> An MLD-fabricated membrane can have high uniformity with minimal defects. Furthermore, transport resistance can be reduced by using a minimal MLD layer thickness and precise functionalization. Similar approaches using ALD have also been employed to fabricate composite polymeric membranes with enhanced properties.<sup>15,16</sup> These modified membranes may be useful for water purification.<sup>17,18</sup>

Current membrane technology for applications such as water treatment utilizes composite membranes. These membranes consist of a thin dense polymer layer on top of a much thicker porous support. These thicker porous supports are typically polysulfone or polyethersulfone (PES) polymers. The thin dense polymer layer is often a cross-linked polyamide fabricated by interfacial polymerization.<sup>19,20</sup> Control of polymer layer thickness, interstitial voids, and nanopores is difficult using interfacial polymerization.<sup>21</sup>

Performing MLD on porous substrates presents a number of challenges. Porous substrates have high aspect ratios and previous ALD studies have shown that conformal deposition requires careful control of the reaction conditions.<sup>22–24</sup> In addition, conformal deposition may not be desired because conformal growth will eventually fill and block the pores of the porous support as shown in Fig. 1(a).<sup>25,26</sup> The conductance of the membrane will be progressively lowered as the pore diameters are reduced by the MLD cycles.<sup>27–29</sup>

This paper describes a method to deposit continuous polymer MLD films only on top of porous substrates using a combination of plasma-enhanced atomic layer deposition (PE-ALD) and MLD.

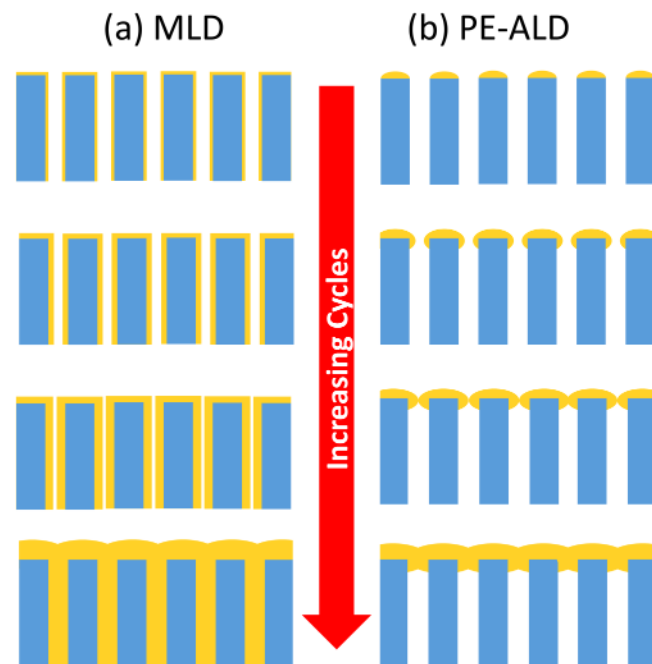


**FIG. 1.** Illustration of (a) MLD and (b) PE-ALD on porous substrates vs increasing number of cycles.

PE-ALD is a subcategory of ALD that utilizes plasma-generated chemical species as a precursor in the ALD process.<sup>30</sup> PE-ALD can cap the pores of porous supports because the PE-ALD is limited to the top of the pores as shown in Fig. 1(b).<sup>31–33</sup> PE-ALD is confined to the top because the transmission of active plasma species into high aspect ratio pores is restricted by surface recombination loss within the pores.<sup>34</sup> Diffusion-limited kinetics can also localize the PE-ALD to the top when the reactive sticking coefficient of the active plasma species is high.<sup>24,34</sup> An MLD film can then be deposited on the continuous PE-ALD capping layer.

The strategy for depositing a continuous polymer film only on top of a porous substrate using PE-ALD and MLD is shown in Fig. 2. This strategy is implemented using porous anodic aluminum oxide (AAO) or PES support substrates with nanometer-scale pore diameters. The pores of the substrate are capped using  $\text{Al}_2\text{O}_3$  PE-ALD. A polyamide MLD film is then deposited on the  $\text{Al}_2\text{O}_3$

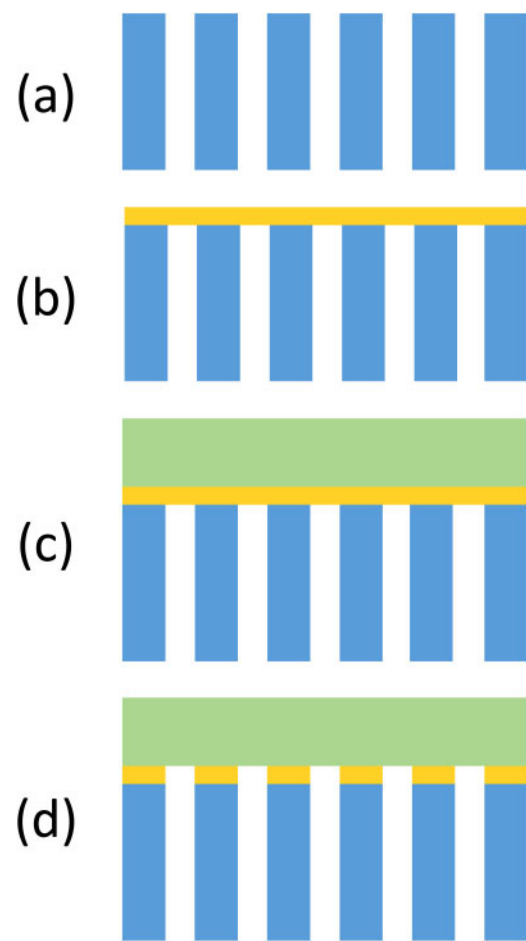


**FIG. 2.** Schematic of the strategy used to deposit a continuous polymer MLD film on top of a porous substrate. (a) Initial porous substrate. (b) PE-ALD on porous substrate for pore capping. (c) MLD on the continuous PE-ALD capping layer. (d) Backside etching of pore caps to obtain permeable membrane.

pore capping layer. The pore caps can then be removed using an etching solution applied from the backside of the membrane.<sup>35</sup> The result is a thin continuous MLD film attached to the top of the porous substrate. Alternative methods based on film transfer techniques can also achieve continuous polymer films on top of porous supports.<sup>36</sup> However, these polymers films are not bonded as securely and are difficult to scale.<sup>37</sup>

One difficulty with the strategy shown in Fig. 2 is that the backside etching can also remove the Al<sub>2</sub>O<sub>3</sub> layer underneath the polyamide MLD film depending on the etching time. Removal of the Al<sub>2</sub>O<sub>3</sub> layer allows the polyamide MLD film to detach from the underlying support. The polyamide MLD film can be more firmly anchored to the porous support if there are cracks in the Al<sub>2</sub>O<sub>3</sub> layer prior to the MLD. In this case, the MLD can coat both the Al<sub>2</sub>O<sub>3</sub> layer and the porous support through the cracks in the Al<sub>2</sub>O<sub>3</sub> layer. The MLD film deposited on the porous support acted to anchor the MLD film to the porous support.

## II. EXPERIMENT

### A. Porous substrates

Two porous substrates were examined in this study: ceramic AAO membranes and PES membranes. The AAO membranes (InRedox) were used as a model porous ceramic substrate.<sup>24</sup> The anisotropic AAO membrane is defined by a 1.5- $\mu\text{m}$ -thick active layer with 10 nm pores and 60- $\mu\text{m}$ -thick support layer with 100 nm diameter pores. The pore concentration and porosity in the active layer were  $1.6 \times 10^{11} \text{ cm}^{-2}$  and 12%, respectively. Sample diameters were 13 mm.

PES ultrafiltration membranes (MilliporeSigma) were utilized as a model flexible porous polymer substrate. Like the AAO membranes, the PES membranes were asymmetric with an active layer containing pores. The range of pore sizes in the active layer was between 5 and 50 nm. The glass transition temperature of PES is 220 °C. The PES membranes had no fiber support.

### B. Plasma-enhanced atomic layer deposition

The deposition of Al<sub>2</sub>O<sub>3</sub> pore caps by PE-ALD was performed at room temperature in a custom-built remote plasma ALD reactor.<sup>38</sup> The remote plasma system was able to minimize sample etching and heating.<sup>39</sup> Samples were exposed to sequential doses of trimethylaluminum (TMA) (97%, Aldrich), nitrogen (N<sub>2</sub>) (4.8 grade, AirGas), and oxygen plasma (4.4 grade O<sub>2</sub> gas, AirGas). The nitrogen dose served to purge the TMA from the reactor. No purge step was utilized after the oxygen plasma step because of the short lifetime of the reactive radical species in the oxygen plasma.<sup>40</sup> Exposure times of TMA/N<sub>2</sub>/oxygen plasma were 3, 1, and 2 s, respectively, followed by pumping times of 45, 25, and 18 s, respectively. The static exposure pressures of TMA and N<sub>2</sub> were 0.75 and 1.0 Torr, respectively. Short exposures to the RF plasma are sufficient for generating active species and to minimize heat shrinkage of the polymer resulting from heating.<sup>41</sup> All the reactions were performed at the ambient temperature of 23 °C.

The 200 W oxygen plasma was produced by a 2 kW RF Plasma Generator (Paramount HALO 3156300-000A, Advanced Energy). This remote plasma reactor had a reaction volume that

was separated from the plasma source by a gate valve. The measured flow rate of O<sub>2</sub> through the plasma source was 3.0 SCCM. The pressure of oxygen during oxygen plasma exposures was 45 mTorr above base pressure.

The AAO samples were mounted normal to the plasma flux at a distance of 23 cm from the edge of the RF coils. The PES samples were placed parallel to the plasma flux on top of a removable metal tray that bisected the tube of the reactor. Silicon coupons were placed in the reactor next to the porous samples to serve as a witness of the PE-ALD growth.

### C. Spatial molecular layer deposition

A spatial MLD reactor was utilized to deposit the polymer MLD films on the porous substrates. The design and operation of this rotating cylinder reactor for ALD or MLD have been detailed elsewhere.<sup>25,26,42–44</sup> Samples were mounted to the inner drum of the spatial MLD system using Kapton adhesive. The adhesive was applied to all sides of the porous samples to prevent backside deposition. The system was maintained at near-isothermal conditions within a custom convection oven that contained the dosing lines and valves.

The polymer MLD was conducted using *m*-phenylenediamine (MPD) (99%, Sigma Aldrich) and trimesoyl chloride (TMC) (98%, Sigma Aldrich) as the reactants.<sup>42</sup> The two precursor zones in the spatial MLD reactor were individually dosed with MPD and TMC.<sup>42</sup> All chemicals were stored in stainless steel containers within the convection oven. Each precursor was connected to the reactor by two bellows globe valves on either side of a bellows needle valve for metering flow.

The MLD reactions were performed at a drum rotation rate of 5 rpm. This rotation rate corresponds to a 1.2 s residence time in the reactive dose zones and a 4.8 s residence time in the purging zones. The reaction temperature was 130 °C. Nitrogen purge gas (4.8 grade, Airgas) was maintained at a flow rate of 200 SCCM and established a base pressure of 1.0 Torr. Precursor flow was manually adjusted to add 200 mTorr above the base pressure. This pressure was measured for each dosing line. A silicon coupon was also placed in the reactor to serve as a witness substrate for thickness measurements.

### D. Backside etching of AAO pore caps

The Al<sub>2</sub>O<sub>3</sub> PE-ALD on AAO samples was performed to study the ability of Al<sub>2</sub>O<sub>3</sub> PE-ALD to cap the pores and then the ability of the NaOH etching to remove the pore caps. After the Al<sub>2</sub>O<sub>3</sub> PE-ALD films were deposited on the AAO porous supports, the backside of each pore-capped AAO sample was etched with a 0.03M NaOH solution. This solution was prepared with ultrapure water and NaOH pellets (97%, Fisher Chemical). The etching process was designed to etch only from the backside of the samples and ensure repeatable etching conditions. AAO samples with 20 PE-ALD Al<sub>2</sub>O<sub>3</sub> cycles were placed in an AAO holder cell (InRedox). The front side faced a sintered porous metal support disk.

A crossflow of ~0.1 ml/min of the NaOH solution was maintained on the backside of the AAO sample. This crossflow ensured constant solution concentration. The crossflow was pressurized by

an N<sub>2</sub> headspace above the reservoir of the NaOH solution. The N<sub>2</sub> pressure was 5 psi. After the designated times, the NaOH solution was cleared by a flow of N<sub>2</sub> gas. Etching was performed at the ambient temperature of 23 °C. Following each etch, the samples were rinsed in ultrapure water and then dried in an oven at 70 °C.

### E. Etching of PES pore caps

After the PE-ALD and MLD films were deposited on the PES porous supports, samples were prepared using a punch to define a 50 mm diameter. Samples were immersed in a stirred bath of 100 ml of 0.03M NaOH solution. The PES samples were fully immersed in the etching solution with the MLD layer on top of the Al<sub>2</sub>O<sub>3</sub> pore caps. The MLD layer protected the Al<sub>2</sub>O<sub>3</sub> capping layer from etching from the top side. Samples were etched for 20 or 40 min and then rinsed with ultrapure water. The samples were air dried at room temperature before measuring the gas permeance.

### F. Spectroscopic ellipsometry

Spectroscopic ellipsometry measured film thicknesses on the silicon witness coupons using a spectroscopic ellipsometer (M-2000, J.A. Woollam Co., Inc.) and modeling software (COMPLETTEASE, J.A. Woollam Co., Inc.). Measurements of the Al<sub>2</sub>O<sub>3</sub> film thicknesses were performed at a 70° incident angle. The spectra were fit using a Cauchy model. Measurements of the polyamide MLD film were performed at three angles: 50°, 60°, and 70°. The spectra were fit with two Gaussian oscillator curves and an anisotropic index difference in the z axis with parameters developed from multisample analysis.

### G. Gas permeance measurements

Gas permeance measurements were performed using a custom-built system comprised of a compressed nitrogen tank sourcing pressure to a dead-end membrane flow cell. Commercial membrane cells were used to hold the AAO (InRedox, AAO Membrane Holder) and PES samples (Sterlitech, HP4750). Pressure was controlled with a regulator and measured with a pressure transducer (OMEGA, PX309-300G5 V). Flow rate was measured with a mass flow controller in the read operation (Alicat, MC-100SCCM-D).

To improve the handling and integrity of AAO samples, each AAO disk was adhered to a ring of Kapton adhesive. These rings had a 10 mm inner diameter that overlapped and sealed to the 13 mm AAO disks. The outer diameter of these Kapton rings was 25 mm and provided a sealing surface for the O-ring of the membrane holder to prevent the fracture of the brittle AAO material. For PES, gas permeance measurements were conducted on 50 mm diameter samples. During these gas permeance experiments, the samples were backed by a sintered porous metal disk with the active layer facing upstream. Mass flow measurements were performed using a pressure drop of 100 psi. Gas permeance was calculated as volumetric flow rate per pressure drop per unit area.

### H. Scanning electron and optical microscopy

Images of fractured samples were obtained with scanning electron microscopy (SEM) using a Hitachi SU3500 at 30 kV accelerating voltage and a working distance of 11–28 mm. A 1 nm layer of Au was sputtered onto the samples to minimize the effects of

sample charging. All other SEM imaging was performed using a Zeiss GeminiSEM 500 at 3 kV accelerating voltage and a working distance of 3–5 mm. A 1–3 nm layer of Au–Pd was sputtered onto these samples to minimize the effects of sample charging. Additional imaging was performed using an optical microscope (Micromanipulator, 6000) with standard optics (Mitutoyo, Plan Apo Objective).

## III. RESULTS AND DISCUSSION

### A. Al<sub>2</sub>O<sub>3</sub> PE-ALD

Figure 3 shows the growth of Al<sub>2</sub>O<sub>3</sub> PE-ALD films on silicon witness substrates using TMA and oxygen plasma at an ambient temperature of 23 °C. Linear growth was observed with a growth per cycle of 2.4 Å/cycle. This growth rate is higher than the earlier reported growth rate of 1.7 Å/cycle at 25 °C.<sup>45</sup> There was a short nucleation period of two PE-ALD cycles. The oxygen plasma exposures were limited to 2 s. Longer plasma exposure times led to surface corrosion effects. Short exposure times also assisted in limiting the depth of the PE-ALD deposition within the pores.<sup>24,31,32,34</sup>

The PES sheets with dimensions of 25 × 5 cm were too large relative to the size of the cylindrical reaction chamber to be positioned normal to the plasma flux. Consequently, the PES sheets were loaded lengthwise into the reactor with their surfaces parallel to the plasma flux. To test for uniform deposition, 15 silicon coupons were placed in a grid at various points along the axis of the reactor and off-axis at the midplane of the reaction tube. After 85 PE-ALD cycles, the relative standard deviation of measured thicknesses for the various locations in the reactor was 1.5% with no apparent trends. These results indicate that the Al<sub>2</sub>O<sub>3</sub> PE-ALD films should be uniform on the surface of the PES sheets.

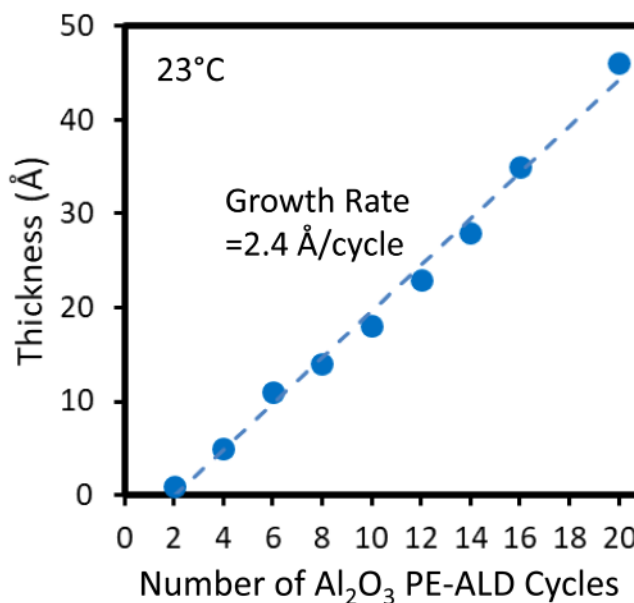


FIG. 3. Al<sub>2</sub>O<sub>3</sub> film thickness vs number of Al<sub>2</sub>O<sub>3</sub> PE-ALD cycles using TMA and oxygen plasma as the reactants. Al<sub>2</sub>O<sub>3</sub> PE-ALD growth rate is 2.4 Å/cycle.



The TMA precursor is soluble in PES and can infiltrate the bulk of the membrane material.<sup>46</sup> However, deposition in the polymer membrane is unlikely because oxygen radicals cannot easily diffuse into PES. Radical species experience recombination on surfaces.<sup>34</sup> Rather than absorbing into the polymer, oxygen plasma species induce bond scissions at the surface of PES substrates.<sup>47,48</sup> This study observed that a PES sample exposed to oxygen plasma for many minutes was severely cracked, thinner, and brittle.

### B. Gas permeance versus number of PE-ALD cycles

Al<sub>2</sub>O<sub>3</sub> PE-ALD was performed on AAO samples to evaluate the ability of Al<sub>2</sub>O<sub>3</sub> PE-ALD to cap the pores of the AAO samples. Figure 4 shows the relationship between the gas permeance and the number of Al<sub>2</sub>O<sub>3</sub> PE-ALD cycles. There was a progressive reduction in gas permeance with increasing number of PE-ALD cycles. These results illustrate that Al<sub>2</sub>O<sub>3</sub> PE-ALD can tune the conductance of the AAO samples. After 16 PE-ALD cycles, the flow of N<sub>2</sub> through the AAO membrane was below the measuring capacity. The measured Al<sub>2</sub>O<sub>3</sub> deposition thickness on the silicon witness wafers after 16 PE-ALD cycles was 3.5 nm.

If the AAO membranes had a pore diameter of 10 nm, then the pores should have required an Al<sub>2</sub>O<sub>3</sub> PE-ALD thickness of 5 nm to seal the pores. In contrast, Fig. 4 shows that the pores closed after 3.5 nm of the measured PE-ALD growth. This difference may be attributed to inaccuracies in the measurement of the pore diameters in the AAO membrane. Furthermore, a nucleation period was observed during the first two PE-ALD cycles on the silicon substrates in Fig. 3. This nucleation period may not exist for

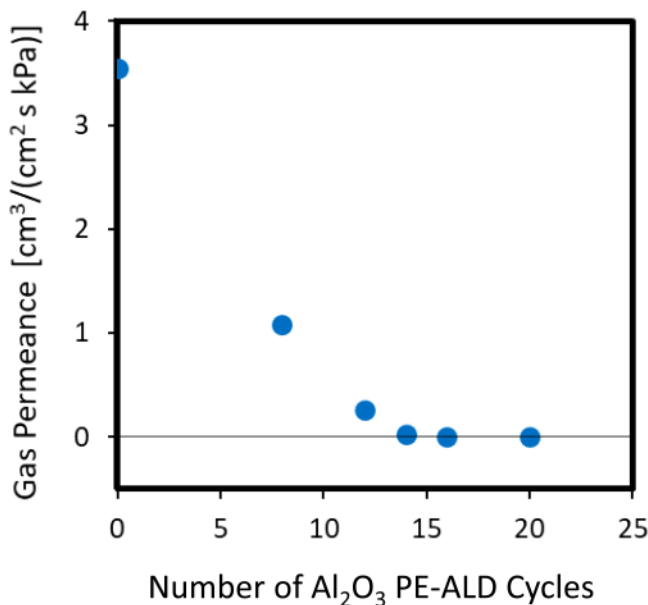


**FIG. 4.** Gas permeance vs number of Al<sub>2</sub>O<sub>3</sub> PE-ALD cycles for an AAO membrane.

the AAO substrates. Consequently, the PE-ALD films on AAO may have been slightly thicker than on the witness silicon wafers.

Figures 5(a) and 5(b) display SEM images of the active side of unprocessed AAO membranes and AAO membranes capped with 20 Al<sub>2</sub>O<sub>3</sub> PE-ALD cycles, respectively. A visual change in the surface morphology is apparent between these two samples. The capped AAO surface had fewer visible openings than the bare AAO surface. Although the capped surface still appears to have open surface pores, the measured gas permeance shown in Fig. 4 was below the detection limit after 20 PE-ALD cycles, indicating full pore closure.

### C. Backside etching of Al<sub>2</sub>O<sub>3</sub> pore caps

An AAO membrane coated with 20 Al<sub>2</sub>O<sub>3</sub> PE-ALD cycles was then etched from the backside using a 0.03M NaOH solution to remove the Al<sub>2</sub>O<sub>3</sub> PE-ALD pore caps from the top of the AAO membrane. Figure 5(c) shows an SEM image of the top side of the AAO membrane sample after 3 min of etching. The morphology of the active layer was similar to the morphology of the AAO sample after 20 Al<sub>2</sub>O<sub>3</sub> PE-ALD cycles shown in Fig. 5(b). The active side was still unaffected because no breakthrough has occurred after 3 min of etching.

Figure 6 displays the effect of etch time on the gas permeance of the AAO sample coated with 20 Al<sub>2</sub>O<sub>3</sub> PE-ALD cycles. The dotted line shows the permeance of the unprocessed AAO sample with no PE-ALD cycles. The gas permeance increased with the etch time. After a 300 s etch time, the measured permeance of the AAO sample coated with 20 Al<sub>2</sub>O<sub>3</sub> PE-ALD cycles reached the

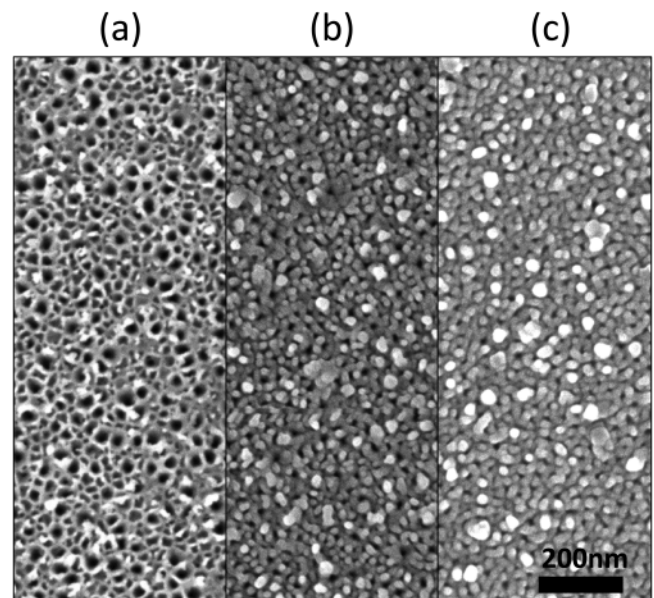


**FIG. 5.** SEM images of active side of AAO membranes. (a) Unprocessed AAO. (b) AAO with 20 cycles of Al<sub>2</sub>O<sub>3</sub> PE-ALD. (c) AAO with 20 cycles of Al<sub>2</sub>O<sub>3</sub> PE-ALD after 3 min of backside etching with 0.03M NaOH.

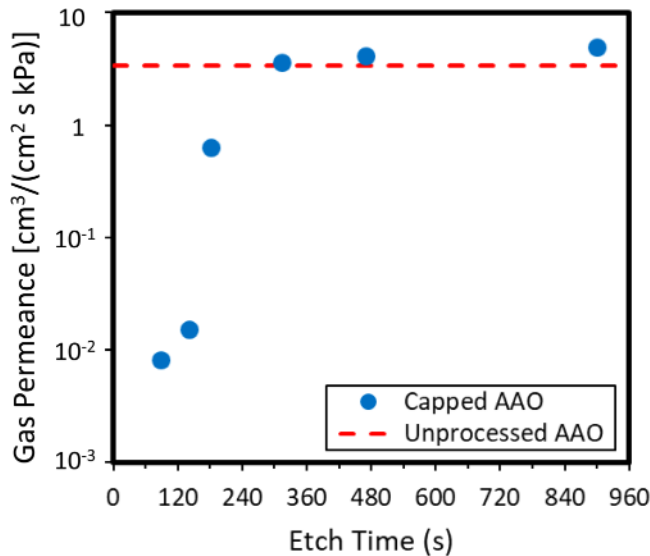


FIG. 6. Gas permeance vs etch time for AAO membranes capped with 20 cycles of Al<sub>2</sub>O<sub>3</sub> PE-ALD after different etching times using 0.03M NaOH.

permeance of an unprocessed AAO sample. The permeance then remained at the permeance of an unprocessed AAO for even longer etch times. The relatively steep slope of the gas permeance over the first 300 s etch times is attributed to the removal of the Al<sub>2</sub>O<sub>3</sub> PE-ALD pore caps. The slight increase of the gas permeance for longer etch times may be caused by the widening of the pores in the original AAO sample.<sup>35</sup>

These results confirm that the Al<sub>2</sub>O<sub>3</sub> PE-ALD layer was limited to the top of the porous AAO substrate. In addition, there was minimal Al<sub>2</sub>O<sub>3</sub> PE-ALD growth inside the pores. The Al<sub>2</sub>O<sub>3</sub> PE-ALD pore capping layer could be controllably removed without compromising the original AAO sample. Based on these results, this method should be useful for the addition of Al<sub>2</sub>O<sub>3</sub> PE-ALD pore caps and their removal from porous substrates using backside etching.

#### D. Pore capping of PES membranes

PES membranes were also coated with Al<sub>2</sub>O<sub>3</sub> PE-ALD to cap the pores on the surface of the PES membrane. Figure 7 displays a progression of SEM images that reveal the effect of the Al<sub>2</sub>O<sub>3</sub> PE-ALD cycles on the PES membrane. The unprocessed PES membrane is shown in Fig. 7(a). This unprocessed PES membrane had surface pores with diameters ranging from 5 to 50 nm. In comparison with the AAO substrates shown in Fig. 5(a), the pores in the PES membrane had a broader size distribution. Figure 7(b) shows that very few surface pores were visible after only ten cycles of Al<sub>2</sub>O<sub>3</sub> PE-ALD. With subsequent PE-ALD cycles, the surface pores visibly disappeared with subsequent PE-ALD cycles as illustrated in Figs. 7(c)–7(e) after 20, 70, and 150 PE-ALD cycles, respectively.

The Al<sub>2</sub>O<sub>3</sub> PE-ALD cycles progressively reduced the gas permeance of the PES membranes. Figure 8 shows the relationship

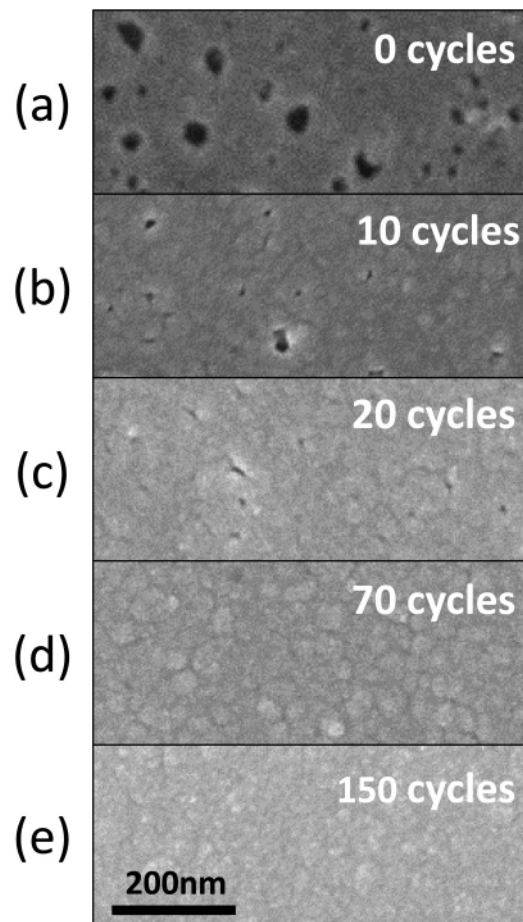


FIG. 7. SEM images of active side of PES membranes. (a) Unprocessed PES. PES membranes with (b) 10, (c) 20, (d) 70, and (e) 150 cycles of Al<sub>2</sub>O<sub>3</sub> PE-ALD.

between gas permeance and the number of Al<sub>2</sub>O<sub>3</sub> PE-ALD cycles applied to the PES samples. The gas permeance decreased with the number of Al<sub>2</sub>O<sub>3</sub> PE-ALD cycles. After 60 or more Al<sub>2</sub>O<sub>3</sub> PE-ALD cycles, the measured gas permeance was  $<2 \times 10^{-3} \text{ cm}^3/(\text{cm}^2 \text{ s Pa})$ . These results are different from the results for the AAO membranes shown in Fig. 4. The pores in the AAO membrane became fully sealed after 16 Al<sub>2</sub>O<sub>3</sub> PE-ALD cycles at an Al<sub>2</sub>O<sub>3</sub> PE-ALD thickness of 3.5 nm. In contrast, the permeance of the PES samples never fell below the detection limit, even after 150 Al<sub>2</sub>O<sub>3</sub> PE-ALD cycles.

This lack of complete blockage of the gas flow is attributed to the cracking of the Al<sub>2</sub>O<sub>3</sub> PE-ALD film. This cracking occurred when placing the Al<sub>2</sub>O<sub>3</sub>-topped PES samples in the measurement cell. Due to the compressive force on the samples from the O-ring seal, fracture of the brittle, ceramic Al<sub>2</sub>O<sub>3</sub> PE-ALD layer occurred against the flexible PES substrate under compression.<sup>49,50</sup> Based on the SEM micrographs in Fig. 7, full pore capping of the PES occurred after >20 PE-ALD cycles. However, the film fracture from the compressive O-ring seal leads to nonzero gas permeance.

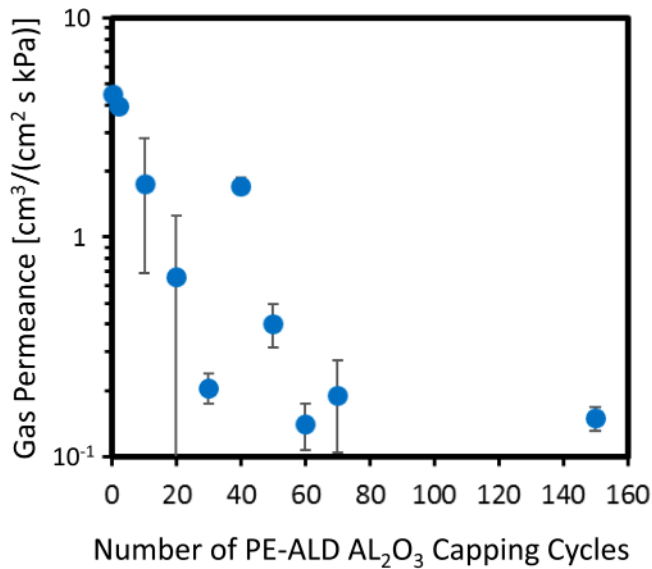


FIG. 8. Gas permeance vs number of Al<sub>2</sub>O<sub>3</sub> PE-ALD cycles for a PES membrane.

The fracture of the Al<sub>2</sub>O<sub>3</sub> PE-ALD layer can be observed by SEM images. Figure 9 shows the SEM image of a PES sample that was prepared with 70 Al<sub>2</sub>O<sub>3</sub> PE-ALD cycles. Figure 9(a) shows the SEM image of the film fracture caused by compression against the O-ring. Figure 9(b) displays an SEM image after the sample was fractured as a result of cutting. Fracturing of the Al<sub>2</sub>O<sub>3</sub> PE-ALD layer on the AAO substrates was not observed because the AAO substrate and the Al<sub>2</sub>O<sub>3</sub> PE-ALD layer have similar flexural properties.

### E. Polyamide MLD-Al<sub>2</sub>O<sub>3</sub> PE-ALD-PES composite membranes

MLD films were also grown on top of PES membranes coated with 40 Al<sub>2</sub>O<sub>3</sub> PE-ALD cycles. The polyamide MLD films had a thickness of 290 nm after 774 cycles at 5 rpm at 130 °C. The growth rate of the polyamide MLD film is 3.7 Å/cycle. This growth rate compares with the growth rate of 4.5 Å/cycle reported earlier using the same reactants at 20 rpm at 115 °C.<sup>42</sup>

Optical micrographs of these composite membranes revealed a number of fractures as displayed in Fig. 10. Most of the fractures likely resulted from differences in the thermal expansion between the Al<sub>2</sub>O<sub>3</sub> layer and the underlying PES membrane.<sup>49,51</sup> Al<sub>2</sub>O<sub>3</sub> has a relatively low thermal expansion coefficient of  $4.2 \times 10^{-6}$  cm/cm K.<sup>50</sup> PES has a much larger thermal expansion coefficient of  $\sim 54 \times 10^{-6}$  cm/cm K.<sup>41,52</sup> The thermal expansion of the PES substrate upon heating for MLD at 130 °C leads to tensile stress in the Al<sub>2</sub>O<sub>3</sub> layer.<sup>49,51</sup>

Earlier work studied thermal Al<sub>2</sub>O<sub>3</sub> ALD films that were grown on Teflon at higher temperatures and experienced a compressive stress upon cooling.<sup>49,51</sup> This compressive stress resulted

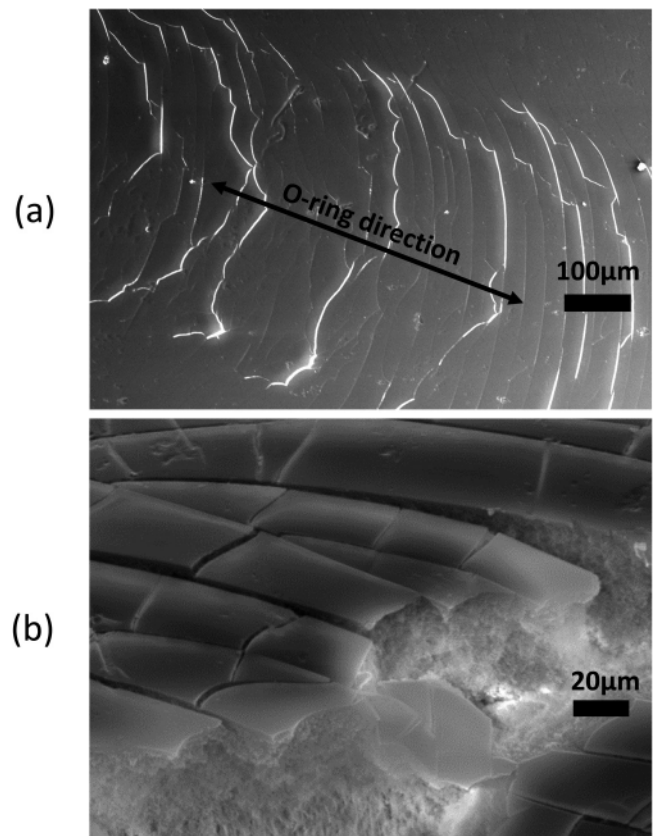


FIG. 9. SEM image of a PES membrane with 70 cycles of PE-ALD Al<sub>2</sub>O<sub>3</sub>. (a) Fracture caused by O-ring compression and (b) fracture caused by scissors cut.

from thermal expansion mismatch between the Al<sub>2</sub>O<sub>3</sub> ALD film and the Teflon substrate. A tensile stress for an Al<sub>2</sub>O<sub>3</sub> ALD film grown at low temperature on a polymer and then heated to a higher temperature is consistent with a compressive stress for an Al<sub>2</sub>O<sub>3</sub> ALD film grown at higher temperature on a polymer and then cooled to a lower temperature.<sup>49,51</sup>

The Al<sub>2</sub>O<sub>3</sub> pore caps were removed from the polyamide MLD-Al<sub>2</sub>O<sub>3</sub> PE-ALD-PES composite membranes using a 20 min exposure in a 0.03M NaOH solution. The thickness of the Al<sub>2</sub>O<sub>3</sub> PE-ALD layers on these PES membranes was 16 nm. The optical micrographs revealed that the MLD layer began to separate from the PES membrane after the dissolution of the Al<sub>2</sub>O<sub>3</sub> pore caps. The optical micrograph displayed in Fig. 11 reveals that the polymer MLD film was buckled after detaching from the underlying PES membrane. An inspection of the optical micrograph also revealed that the polymer MLD film was only anchored to the PES substrate at the lines of fracture in the initial Al<sub>2</sub>O<sub>3</sub> PE-ALD film.

The polyamide MLD film is only attached to the PES substrate through the fractures in the original Al<sub>2</sub>O<sub>3</sub> PE-ALD layer. The polyamide MLD layer was able to anchor itself securely by deposition inside the pores of the PES substrate. This explanation is



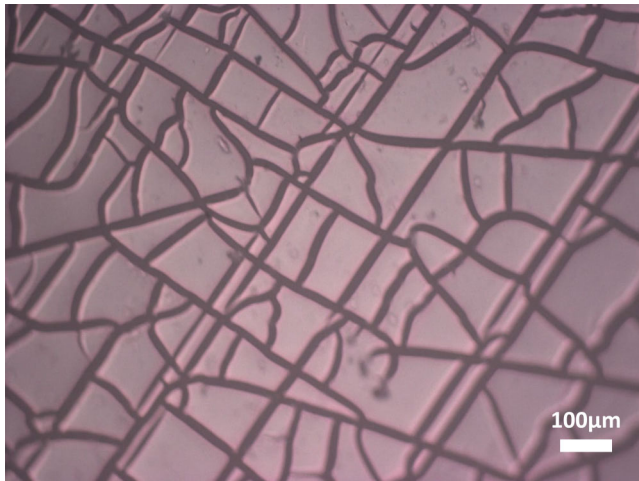


**FIG. 10.** Light microscopy image of a PES membrane coated with a PE-ALD  $\text{Al}_2\text{O}_3$  layer and a polyamide MLD layer. A PE-ALD  $\text{Al}_2\text{O}_3$  layer was deposited at 23 °C using 40  $\text{Al}_2\text{O}_3$  PE-ALD cycles. A polyamide MLD layer was deposited at 130 °C and had a thickness of 290 nm.

supported by the observation that the polyamide MLD- $\text{Al}_2\text{O}_3$  PE-ALD-PES composite membranes displayed no gas permeance prior to removal of the  $\text{Al}_2\text{O}_3$  pore caps by dissolution using the 0.03M NaOH solution. Although many fractures existed in the  $\text{Al}_2\text{O}_3$  PE-ALD layer, polyamide MLD filled the pores in the PES substrate through the cracks in the  $\text{Al}_2\text{O}_3$  PE-ALD layer and inhibited any gas flow.

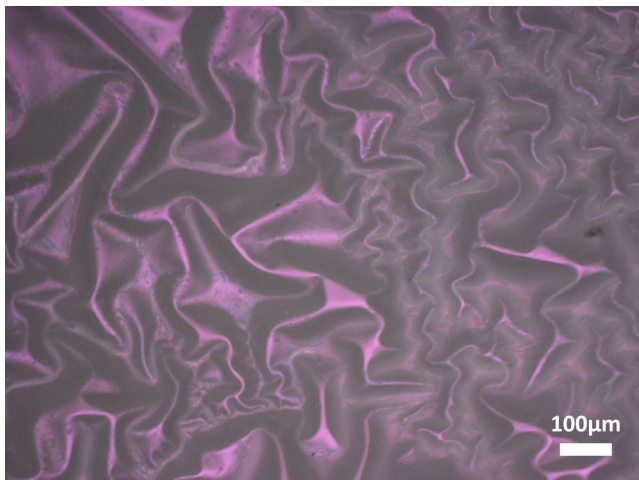


**FIG. 11.** Light microscopy image of a PES sample after 40 cycles of PE-ALD  $\text{Al}_2\text{O}_3$  and then depositing 290 nm of a polyamide MLD film. Image is recorded after 20 min in a 0.03M NaOH solution.

The water permeability of these polyamide MLD- $\text{Al}_2\text{O}_3$  PE-ALD-PES composite membranes was measured using a pressure of 225 psi. Optical micrographs after testing showed that the buckled regions of the polyamide MLD film tore and pulled away from the underlying PES membrane. In addition, the regions in the continuous polyamide MLD film with greater distance between the anchoring lines were more susceptible to failure. This behavior suggested that the polyamide MLD film would be more robust if there were more fracture lines in the initial  $\text{Al}_2\text{O}_3$  PE-ALD layer and more anchoring to the underlying PES substrate.

#### F. Anchoring MLD polymer by fracture of $\text{Al}_2\text{O}_3$ PE-ALD layer

The anchoring of the polyamide MLD film was dependent on the number of fractures in the original  $\text{Al}_2\text{O}_3$  PE-ALD layer. Consequently, the  $\text{Al}_2\text{O}_3$  PE-ALD layer was intentionally fractured prior to MLD. By bending the  $\text{Al}_2\text{O}_3$  PE-ALD-PES samples over a fixed radius, a regular pattern of fractures was produced in the  $\text{Al}_2\text{O}_3$  PE-ALD layer.<sup>49</sup> Bending over an 11.4 mm diameter mandrel produced parallel fractures at a spacing of  $\sim 100\ \mu\text{m}$ . Polyamide MLD on these fractured  $\text{Al}_2\text{O}_3$  PE-ALD layers followed by etching produced the optical micrograph shown in Fig. 12. The anchor lines for the polyamide MLD film are evident at a spacing of  $\sim 100\ \mu\text{m}$ .

Fractures in the  $\text{Al}_2\text{O}_3$  PE-ALD layer could also be produced in both the x and y directions of the PES substrate. Bending over a 3.2 mm diameter mandrel along both sheet axes produced orthogonal fractures at a spacing of  $\sim 50\ \mu\text{m}$  in the  $\text{Al}_2\text{O}_3$  PE-ALD layer. Polyamide MLD on these fractured  $\text{Al}_2\text{O}_3$  PE-ALD layers followed by etching produced the optical micrograph shown in Fig. 13. The

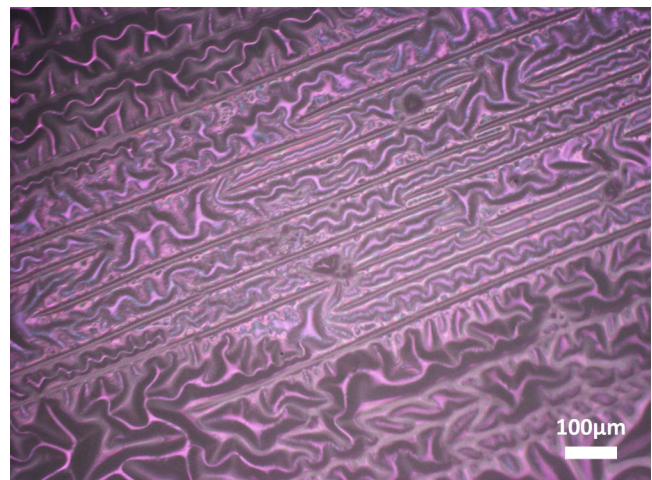


**FIG. 12.** Light microscopy image of a PES sample after 40 cycles of PE-ALD  $\text{Al}_2\text{O}_3$  and then depositing 290 nm of a polyamide MLD film. Fracture in the  $\text{Al}_2\text{O}_3$  film was produced by bending the  $\text{Al}_2\text{O}_3$  film across an 11.4 mm diameter mandrel prior to polyamide MLD. Image is recorded after 20 min in a 0.03M NaOH solution.



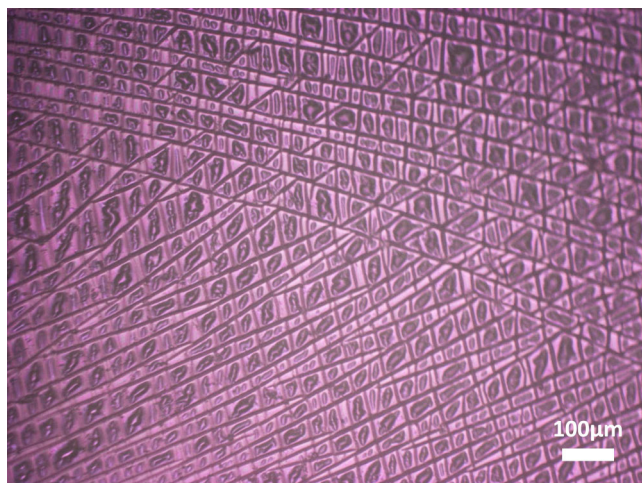


**FIG. 13.** Light microscopy image of a PES sample after 40 cycles of PE-ALD  $\text{Al}_2\text{O}_3$  and then depositing 290 nm of a polyamide MLD film. Fracture in the  $\text{Al}_2\text{O}_3$  film was produced by bending the  $\text{Al}_2\text{O}_3$  film across a 3.2 mm diameter mandrel along both sheet axes prior to polyamide MLD. Image is recorded after 20 min in a 0.03M NaOH solution.

anchor lines for the polymer MLD layer formed a distinctive cross-hatched pattern.

The polyamide MLD- $\text{Al}_2\text{O}_3$  PE-ALD-PES composite membranes with the greater number of anchoring points were the most robust. Samples with larger spacing between anchor points experienced failure more frequently when subjected to pressure. However, the sample shown in Fig. 13 with a polyamide MLD film thickness of 290 nm was impermeable to both nitrogen and water up to 225 psi. Perhaps thinner MLD films are needed for measurable permeability. If permeable MLD films can be demonstrated, then this technique has the potential for producing robust, thin film composite membranes. Such MLD membrane systems could prove useful for a number of important pressure-driven separation applications such as reverse osmosis, gas separation, or pervaporation.

#### IV. CONCLUSIONS

A method to deposit continuous polymer films on top of porous substrates was developed based on PE-ALD and MLD. PE-ALD was first used to cap the pores of the porous substrate. An MLD polymer film was then deposited on the PE-ALD capping layer. This method was demonstrated using AAO and PES porous substrates. This new strategy should be useful for adding polymer MLD films to the surface of porous substrates to create new composite membranes for separation applications.

The experiments on porous AAO substrates revealed that  $\text{Al}_2\text{O}_3$  PE-ALD film growth could cap the pores on top of AAO substrates. Following  $\text{Al}_2\text{O}_3$  PE-ALD film growth, a continuous surface was available for the deposition of a polymer MLD film. The pores could then be reopened by dissolving the  $\text{Al}_2\text{O}_3$  pore caps with sodium hydroxide. Gas permeance measurements confirmed the closure of the pores in AAO membranes coated with

$\text{Al}_2\text{O}_3$  PE-ALD films and the reopening of the pores versus NaOH etch time.

The pores in PES membranes could also be closed using  $\text{Al}_2\text{O}_3$  PE-ALD film growth. However, gas permeance measurements indicated that  $\text{Al}_2\text{O}_3$  PE-ALD film growth did not completely limit gas transmission. The nonzero gas permeance was traced back to the fracture of the  $\text{Al}_2\text{O}_3$  PE-ALD films on the PES membranes during sample testing. Fracture occurred due to compression of the  $\text{Al}_2\text{O}_3$  PE-ALD/PES membrane when making the O-ring seal for subsequent testing.

The fracture of the  $\text{Al}_2\text{O}_3$  PE-ALD film also provided a mechanism to anchor the polyamide MLD film to the PES membrane. The  $\text{Al}_2\text{O}_3$  film fracture allowed the MLD film to attach firmly to the PES porous substrate by MLD deposition in the pores of the PES substrate. After dissolving the  $\text{Al}_2\text{O}_3$  film, the polyamide MLD film remained anchored to the PES substrate through the original fracture lines in the  $\text{Al}_2\text{O}_3$  PE-ALD film. The  $\text{Al}_2\text{O}_3$  PE-ALD film could be intentionally fractured to provide more fracture lines for anchoring the MLD film to the PES substrate. The stability of the polyamide MLD film improved with a smaller spacing between initial fractures in the  $\text{Al}_2\text{O}_3$  PE-ALD film.

#### ACKNOWLEDGMENTS

This research was initiated by the U.S. Department of Energy (DOE) (No. DE-EE0005771) through a subcontract from GE Global Research. The authors thank Robert Gemmer of the Department of Energy for many useful discussions. Continued support for this research was provided from the Laboratory Directed Research and Development Program at Sandia National Laboratories, a multimission laboratory managed and operated by National Technology and Engineering Solutions of Sandia LLC, a wholly owned subsidiary of Honeywell International Inc. for the U.S. Department of Energy's National Nuclear Security Administration under Contract No. DE-NA0003525. Further support was provided by the Membrane Science, Engineering and Technology Center (NSF IUCRC Award IIP No. 1624602) at the University of Colorado Boulder. The authors thank James Redmond, Susan Rempe, Leo Small, Eliot Fang, and John Emery of Sandia National Laboratories for helpful technical discussions. In addition, the authors thank Dmitri Routkevitch of InRedox for supplying AAO samples and Christina Carbrelo of MilliporeSigma for supplying PES samples. The RF plasma system was provided by Dan Carter at Advanced Energy.

#### REFERENCES

- <sup>1</sup>N. M. Adamczyk, A. A. Dameron, and S. M. George, *Langmuir* **24**, 2081 (2008).
- <sup>2</sup>Y. Du and S. M. George, *J. Phys. Chem. C* **111**, 8509 (2007).
- <sup>3</sup>T. Yoshimura, S. Tatsuura, and W. Sotoyama, *Appl. Phys. Lett.* **59**, 482 (1991).
- <sup>4</sup>S. M. George, B. Yoon, and A. A. Dameron, *Acc. Chem. Res.* **42**, 498 (2009).
- <sup>5</sup>S. M. George, *Chem. Rev.* **110**, 111 (2010).
- <sup>6</sup>P. Sundberg, M. Karppinen, *Beilstein J. Nanotechnol.* **5**, 1104 (2014).
- <sup>7</sup>H. Zhou and S. F. Bent, *J. Vac. Sci. Technol. A* **31**, 040801 (2013).
- <sup>8</sup>M. Weber, A. Julbe, A. Ayril, P. Miele, and M. Bechelany, *Chem. Mater.* **30**, 7368 (2018).
- <sup>9</sup>M. Weber, A. Julbe, S. S. Kim, and M. Bechelany, *J. Appl. Phys.* **126**, 041101 (2019).

- <sup>10</sup>T. Sheng, H. Chen, S. Xiong, X. Q. Chen, and Y. Wang, *AIChE J.* **60**, 3614 (2014).
- <sup>11</sup>Z. N. Song, M. Fathizadeh, Y. Huang, K. H. Chu, Y. M. Yoon, L. Wang, W. W. L. Xu, and M. Yu, *J. Membr. Sci.* **510**, 72 (2016).
- <sup>12</sup>S. Xiong, T. Sheng, L. Kong, Z. X. Zhong, J. Huang, and Y. Wang, *Chin. J. Chem. Eng.* **24**, 843 (2016).
- <sup>13</sup>T. Sheng, L. Kong, and Y. Wang, *J. Membr. Sci.* **486**, 161 (2015).
- <sup>14</sup>H. H. Wang, M. J. Wei, Z. X. Zhong, and Y. Wang, *J. Membr. Sci.* **535**, 56 (2017).
- <sup>15</sup>F. Li, L. Li, X. Liao, and Y. Wang, *J. Membr. Sci.* **385–386**, 1 (2011).
- <sup>16</sup>Q. Q. Wang, X. T. Wang, Z. H. Wang, J. Huang, and Y. Wang, *J. Membr. Sci.* **442**, 57 (2013).
- <sup>17</sup>A. Lee, J. W. Elam, and S. B. Darling, *Environ. Sci. Water Res. Technol.* **2**, 17 (2016).
- <sup>18</sup>H. C. Yang, R. Z. Waldman, Z. W. Chen, and S. B. Darling, *Nanoscale* **10**, 20505 (2018).
- <sup>19</sup>K. P. Lee, T. C. Arnot, and D. Mattia, *J. Membr. Sci.* **370**, 1 (2011).
- <sup>20</sup>M. Wilf, “The reverse osmosis process,” in *Desalination: Water From Water*, edited by J. Kucera (Wiley, New York, 2014), p. 155.
- <sup>21</sup>C. L. Kong, M. Kanezashi, T. Yamamoto, T. Shintani, and T. Tsuru, *J. Membr. Sci.* **362**, 76 (2010).
- <sup>22</sup>V. Cremers, R. L. Puurunen, and J. Dendooven, *Appl. Phys. Rev.* **6**, 021302 (2019).
- <sup>23</sup>C. Detavernier, J. Dendooven, S. P. Sree, K. F. Ludwig, and J. A. Martens, *Chem. Soc. Rev.* **40**, 5242 (2011).
- <sup>24</sup>J. W. Elam, D. Routkevitch, P. P. Mardilovich, and S. M. George, *Chem. Mater.* **15**, 3507 (2003).
- <sup>25</sup>K. Sharma, D. Routkevitch, N. Varaksa, and S. M. George, *J. Vac. Sci. Technol. A* **34**, 01A146 (2016).
- <sup>26</sup>J. M. Wallas *et al.*, *ACS Appl. Energy Mater.* **2**, 4135 (2019).
- <sup>27</sup>B. S. Berland, I. P. Gartland, A. W. Ott, and S. M. George, *Chem. Mater.* **10**, 3941 (1998).
- <sup>28</sup>M. A. Cameron, I. P. Gartland, J. A. Smith, S. F. Diaz, and S. M. George, *Langmuir* **16**, 7435 (2000).
- <sup>29</sup>L. Velleman, G. Triani, P. J. Evans, J. G. Shapter, and D. Losic, *Microporous Mesoporous Mater.* **126**, 87 (2009).
- <sup>30</sup>H. B. Profijt, S. E. Potts, M. C. M. van de Sanden, and W. M. M. Kessels, *J. Vac. Sci. Technol. A* **29**, 050801 (2011).
- <sup>31</sup>Y. B. Jiang, N. G. Liu, H. Gerung, J. L. Cecchi, and C. J. Brinker, *J. Am. Chem. Soc.* **128**, 11018 (2006).
- <sup>32</sup>Y. B. Jiang, G. Xomeritakis, Z. Chen, D. Dunphy, D. J. Kissel, J. L. Cecchi, and C. J. Brinker, *J. Am. Chem. Soc.* **129**, 15446 (2007).
- <sup>33</sup>J. Dendooven, D. Deduytsche, J. Musschoot, R. L. Vanmeirhaeghe, and C. Detavernier, *J. Electrochem. Soc.* **157**, G111 (2010).
- <sup>34</sup>H. C. M. Knoop, E. Langereis, M. C. M. van de Sanden, and W. M. M. Kessels, *J. Electrochem. Soc.* **157**, G241 (2010).
- <sup>35</sup>G. Hu, H. Zhang, W. Di, and T. Zhao, *Appl. Phys. Res.* **1**, 78 (2009).
- <sup>36</sup>L. Guio, C. Liu, D. Boures, P. T. Getty, R. Waldman, X. Y. Liu, and S. B. Darling, *J. Visualized Exp.* **148**, e59554 (2019).
- <sup>37</sup>M. Stadermann, S. H. Baxamusa, C. Aracne-Ruddle, M. Chea, S. L. Li, K. Youngblood, and T. Suratwala, *J. Visualized Exp.* **100**, e52832 (2015).
- <sup>38</sup>J. W. Clancey, A. S. Cavanagh, R. S. Kukreja, A. Kongkanand, and S. M. George, *J. Vac. Sci. Technol. A* **33**, 01A130 (2015).
- <sup>39</sup>D. R. Boris, V. D. Wheeler, N. Nepal, S. B. Qadri, S. G. Walton, and C. R. Eddy, *J. Vac. Sci. Technol. A* **38**, 040801 (2020).
- <sup>40</sup>J. L. van Hemmen, S. B. S. Heil, J. H. Klootwijk, F. Roozeboom, C. J. Hodson, M. C. M. van de Sanden, and W. M. M. Kessels, *J. Electrochem. Soc.* **154**, G165 (2007).
- <sup>41</sup>S. J. Yun, J. W. Lim, and J. H. Lee, *Electrochem. Solid State Lett.* **7**, C13 (2004).
- <sup>42</sup>D. J. Higgs, J. W. DuMont, K. Sharma, and S. M. George, *J. Vac. Sci. Technol. A* **36**, 01A117 (2018).
- <sup>43</sup>K. Sharma, R. A. Hall, and S. M. George, *J. Vac. Sci. Technol. A* **33**, 01A132 (2015).
- <sup>44</sup>A. S. Yersak *et al.*, *J. Vac. Sci. Technol. A* **36**, 01A123 (2018).
- <sup>45</sup>S. E. Potts, W. Keuning, E. Langereis, G. Dingemans, M. C. M. van de Sanden, and W. M. M. Kessels, *J. Electrochem. Soc.* **157**, P66 (2010).
- <sup>46</sup>R. Z. Waldman, D. Choudhury, D. J. Mandia, J. W. Elam, P. F. Nealey, A. B. F. Martinson, and S. B. Darling, *JOM* **71**, 212 (2019).
- <sup>47</sup>J. C. Feng, G. Wen, W. Huang, E. T. Kang, and K. G. Neoh, *Polym. Degrad. Stab.* **91**, 12 (2006).
- <sup>48</sup>K. S. Kim, K. H. Lee, K. Cho, and C. E. Park, *J. Membr. Sci.* **199**, 135 (2002).
- <sup>49</sup>S. H. Jen, J. A. Bertrand, and S. M. George, *J. Appl. Phys.* **109**, 084305 (2011).
- <sup>50</sup>D. C. Miller, R. R. Foster, S. H. Jen, J. A. Bertrand, S. J. Cunningham, A. S. Morris, Y. C. Lee, S. M. George, and M. L. Dunn, *Sens. Actuators A Phys.* **164**, 58 (2010).
- <sup>51</sup>S. H. Jen and S. M. George, *ACS Appl. Mater. Interfaces* **5**, 1165 (2013).
- <sup>52</sup>W. A. MacDonald, *J. Mater. Chem.* **14**, 4 (2004).